Black Sea Journal of Engineering and Science
doi: 10.34248/bsengineering.1508116

Open Access Journal
e-ISSN: 2619 – 8991

Research Article
Volume 7 - Issue 5: 1022-1030 / September 2024

FAST AND THERMAL NEUTRON REMOVAL CROSS-SECTION FOR CERAMIC GLASS ALUMINUM OXYNITRIDE

Aydın YILDIRIM[1]*

[1]*Proton Accelerator Facility, Nuclear Energy Research Institute (TENMAK-NÜKEN), 06980, Ankara, Türkiye*

Abstract: This study investigates the effectiveness of transparent aluminum oxynitride (AlON) in neutron shielding, focusing on both fast and thermal neutrons. Using conventional radiation attenuation parameters, the macroscopic neutron removal cross-sections of AlON were calculated for varying neutron energies and material thicknesses. The Geant4 simulation toolkit was employed to model and analyze the neutron interactions with AlON. The results indicate that AlON exhibits a high neutron shielding capacity for fast neutrons (2 MeV), with transmission factor values ranging from 0.783 to 0.260 for material thicknesses between 1 and 10 cm. These values are nearly identical to those for water, which range from 0.782 to 0.257, highlighting AlON's comparable performance. However, for thermal neutrons, AlON's performance was less effective, only surpassing lead but not concrete or water. The findings suggest that while AlON is highly effective for fast neutron shielding, it may require complementary materials to adequately shield thermal neutrons. This could involve using AlON in combination with other materials to create a more comprehensive neutron shielding solution. AlON shows significant potential as a neutron shielding material, particularly for fast neutrons. Its integration with additional shielding materials could enhance its overall effectiveness, making it suitable for various nuclear and radiation protection applications.

Keywords: Neutron, Attenuation, Shielding, Geant4, Cross-section

***Corresponding author:** Proton Accelerator Facility, Nuclear Energy Research Institute (TENMAK-NÜKEN), 06980, Ankara, Türkiye
E mail: aydin.yildirim@tenmak.gov.tr (A. YILDIRIM)
Aydın YILDIRIM https://orcid.org/0000-0003-2141-5355

Received: July 01, 2024
Accepted: September 08, 2024
Published: September 15, 2024

Cite as: Yıldırım A. 2024. Fast and thermal neutron removal cross-section for ceramic glass aluminum oxynitride. BSJ Eng Sci, 7(5): 1022-1030.

1. Introduction

Although encounters with neutron sources in daily life are relatively rare, the highly destructive nature of neutrons makes them significantly more hazardous than the more commonly encountered gamma rays. Moreover, neutrons are frequently utilized in nuclear reactors, accelerator facilities, and various industrial applications, where they can generate high fluxes. The high penetrative capability of neutrons, due to their lack of charge, necessitates enhanced and complicated protective measures for radiation workers operating in environments with neutron sources (Kim et al., 2014; Lakshminarayana et al., 2022; Alomayrah et al., 2024; Reda et al., 2024).

Given the increasing need for more effective radiation shielding, there is considerable motivation to develop new materials that surpass traditional methods in reducing biological damage (ALMisned et al., 2021; ALMisned et al., 2024a; Alzahrani et al., 2024a; Alzahrani et al., 2024b; Alzahrani et al., 2024c; Özdoğan et al., 2024). Advances in material science hold promise for innovative shielding solutions that can provide superior protection against neutron radiation (Al-Buriahi et al., 2020; ALMisned et al., 2024b, Alrowaili et al., 2024). For instance, Ali et al. (2024), investigated the use of unglazed ceramic materials in Boron Neutron Capture Therapy (BNCT), highlighting their dual effectiveness in both gamma attenuation and neutron beam shaping. Their study emphasized the potential of ceramics doped with Pb and Ba, which were found to attenuate gamma radiation without significantly affecting the neutron flux, aligning with International Atomic Energy Agency (IAEA) recommendations. Additionally, research by Katubi et al. (2024), explored the neutron and charged particle attenuation properties of Apatite-Wollastonite (AW) glass ceramics doped with B_2O_3. Their findings suggest that these materials are particularly suitable for absorbing fast and thermal neutrons, with fast neutron removal cross-section (FNRC) values measured at 0.0913, 0.0972, and 0.1024 for AW, AW-B10, and AW-B20 samples, respectively. The study indicates potential applications in neutron and ion beam therapy. Similarly, Zayed et al. (2024), studied the gamma and neutron shielding properties of heavy minerals such as hematite and barite. Their results revealed that while barite is superior in gamma attenuation, hematite excels in thermal neutron shielding, outperforming barite by 210%. However, barite demonstrated better performance for fast neutrons, illustrating the importance of material selection based on the specific type of radiation encountered.

As space travel becomes an increasingly discussed and attainable venture, the exposure of astronauts and space

travelers to cosmic ray-induced neutrons is expected to rise. The challenging space environment, with its heightened levels of neutron radiation, emphasizes the critical importance of advancing neutron shielding technologies (Tellili et al., 2014; Kaçal et al., 2019; Cherkashina et al., 2024). In the coming years, the necessity for effective neutron shielding will become even more pronounced, highlighting the urgency of research and development in this field.

Current shielding methods often rely on materials like boron, polyethylene, and heavy metals, which, while effective, come with limitations such as weight and material degradation over time (Singh and Badiger, 2014; Singh et al., 2014; Pavlenko et al., 2015; Fahmi et al., 2024). Novel materials, including polymer composites and nanomaterials, are being investigated for their potential to provide lighter and more effective neutron shielding (Pianpanit and Saenboonruang, 2024; Reda et al., 2024). Research into these advanced materials suggests they could offer substantial improvements in shielding efficiency, potentially revolutionizing protective measures in both terrestrial and extraterrestrial environments.

Aluminum oxynitride (AlON) is a material that finds numerous applications due to its excellent mechanical properties and optical transparency in the visible spectrum. AlON is produced by combining Al_2O_3 with AlN and is typically represented by the formula $Al_{(64+x)/3}O_{(32-x)}N_x$, where x can range from 0 to 8. Studies have shown that when x equals 5, the resulting aluminum oxynitride ($Al_{23}O_{27}N_5$) achieves its most stable and stoichiometric phase (Li et al., 2024). Some of the material properties of AlON, as reported by Salifu and Olubambi (2023), include a density of 3.67 g/cm^3, 80% transparency from the near-ultraviolet through the visible to the near-infrared regions, high durability, stability up to 1200 °C, three times the hardness of steel of the same thickness, scratch resistance, and excellent refractive index, along with large-scale homogeneity (Salifu and Olubambi, 2023). More generally, the mechanical and optical properties of AlON are summarized in Table 1 and Table 2.

Considering these mechanical and optical characteristics, AlON presents numerous potential applications. It could replace traditional glass in a range of products, from smartphone screens to automotive components. Moreover, AlON could play a significant role in the emerging space travel industry. It might be used in spacecraft windows, exterior coatings for radiation shielding and thermal insulation, protection of electronic equipment against cosmic radiation, and in astronaut suits during space missions or extravehicular activities. Additionally, AlON could be critical in protecting solar cells from radiation without obstructing visible light, which is essential for space exploration. In environments like the lunar surface, where the atmosphere is absent or extremely thin, and cosmic radiation can directly reach the surface, AlON could be suitable as a construction material. Its mechanical properties, comparable to concrete, and its optical characteristics make it particularly useful for transparent structural components.

Table 1. Some mechanical properties of the aluminum oxynitride (Ramisetty et al., 2013, Salifu and Olubambi, 2023)

Property	Value
Young Modulus	334 GPa
Poisson's Ratio	0.24
Knoop Hardness	1800 kg/mm^2
Shear Modulus	135 GPa
Compressive Strength	2.68 GPa
Fracture Toughness	2 MPa/m$^{1/2}$
Flexural Strength	0.38 – 0.7 GPa
Weibull Modulus	8.7
Thermal Conductivity at 25 °C	12.6 W/(mK)
Thermal Expansion Coefficient (30 – 900 °C)	7.5 $\times 10^{-6}$K^{-1}
Thermal Shock Resistance, $R' = \frac{\sigma(1-\upsilon)k}{\alpha E}$	1.2

Table 2. Some optical properties of the aluminum oxynitride (Ramisetty et al., 2013, Salifu and Olubambi, 2023)

Property	Value
Range of Transmission Wavelength	334 GPa
Typical clarity in the visible range	0.24
Typical haze in visible range	1800 kg/mm^2
Absorption coefficient at a wavelength of 3.39 μm	135 GPa
Refractive index at 0.5 μm wavelength	2.68 GPa
Typical transmittance (without AR coatings) in the visible range	2 MPa/m$^{1/2}$
Optical homogeneity achieved in a (15 in × 25 in) part having 3.4 in aperture	0.38 – 0.7 GPa
Weibull Modulus	8.7
Total integrated optical scatter at a wavelength of 0.64 μm, and sample thickness of ~5 mm	12.6 W/(mK)
dn/dT in the wavelength range 3 - 5 μm	7.5 $\times 10^{-6}$K^{-1}

Given these attributes, it is evident that AlON would be highly useful in neutron shielding applications if it also provides good radiation protection. Previous study indicating AlON's effective gamma radiation shielding suggests that its neutron shielding performance warrants investigation (Yıldırım, 2024). In this study, Yıldırım

(2024), investigated the gamma-ray shielding capabilities of AlON and presented the following results. As evidenced by the findings of the study, while AlON exhibits superior gamma-ray shielding properties compared to Ordinary Portland Concrete in its undoped form, its efficacy does not surpass that of lead. The mass attenuation coefficients (MACs) for AlON have been reported to range between 2×10^{-2} and $2 \times 10^{3}\ cm^2/g$. Furthermore, the study compared AlON with commercially available lead-equivalent glasses (e.g., RS-253, RS-253-G18, RS-323-G19, RS-360, RS-250), demonstrating that AlON offers superior shielding compared to non-lead alternatives, while exhibiting comparable performance to lead-containing options, particularly at higher energies. In addition to its potential applications in space, AlON's glass-like structure and transparency in the visible range make it a promising candidate for use as a lead-equivalent glass in radiation shielding, particularly in contexts such as nuclear power plants and healthcare facilities.

The aim of this study is to investigate the shielding performance of aluminum oxynitride against fast and thermal neutrons. The study proceeds as follows: Section 2 describes the interaction of neutrons with matter and discusses neutron shielding parameters and their calculation methods. Section 3 presents the results obtained for fast and thermal neutrons, comparing AlON's performance with traditional shielding materials and discussing its neutron shielding effectiveness. The final section summarizes the study and lists the conclusions.

2. Materials and Methods

2.1 Theoretical Calculations

In this study, the effective neutron removal cross-section of transparent aluminum oxynitride for fast and thermal neutrons was investigated using Geant4 simulations. The cross-section discussed here is not the true interaction probability cross-section but a useful parameter that can be calculated for materials with insufficient hydrogen content. It is generally lower than the true cross-section, approximately two-thirds of its value.

Neutrons interact with the medium primarily through absorption and scattering. The total cross-section (σ_T) is expressed as the sum of the absorption cross-section (σ_A) and the scattering cross-section (σ_S). The relationship between these cross-sections is outlined below (equation 1):

$$\sigma_T = \sigma_A + \sigma_S \tag{1}$$

To calculate the total macroscopic cross-section for a compound or mixture, we use the formula (equation 2):

$$\Sigma_T = \sum_i N_i \tag{2}$$

In this equation, N_i represents the number of nuclei per unit volume of the i_th element in the mixture (Akyıldırım, 2019). For the macroscopic neutron removal cross-section (Σ_R), the calculation is performed using (equation 3):

$$\Sigma_R = \sum_i \rho_i \tag{3}$$

Here, ρ_i is the density of the i_th component, and refers to the neutron removal cross-section of the i_th component. Extending this to a material comprising multiple components, the generalized macroscopic neutron removal cross-section (Σ_R) can be determined as follows (equation 4):

$$\Sigma_{R_S} = \sum_{c=1}^{n} \rho_c (\Sigma_R/\rho)_c = \sum_{c=1}^{n} (F_w)_c \rho_S \tag{4}$$

In this expression, ρ_c denotes the density of the c-th component, $(\Sigma_R/\rho)_c$ signifies the mass removal cross-section of the c_th component, ρ_S is the overall density of the material, and $(F_w)_c$ represents the weight fraction of the c_th component (El-Khayatt, 2010; Gaylan et al., 2021).

In this study, the cross-section to be calculated is the macroscopic removal cross-section, based on the principle of measuring the fraction of incident neutrons that remain unaffected after passing through the material. This calculation is quite similar to the gamma attenuation coefficient and can be computed using the equation given below (equation 5):

$$I = I_0 e^{-\Sigma t} \tag{5}$$

Here, I_0 represents the number of incident neutrons, while I denotes the number of neutrons that pass through the material without interaction. The parameter t in equation 5 refers to the thickness of the material the neutrons traverse, and $\sum$ corresponds to the Σ_R parameter shown in equations 1 - 4. Another useful parameter for discussing equation 5 in the context of neutrons is the Transmission Factor (TF), defined by the equation below (equation 6):

$$TF = \frac{I}{I_0} \tag{6}$$

When considering equations 5 and 6, a relationship between TF and the neutron shielding effectiveness of the material can be observed; the smaller the TF, the better the material's neutron shielding capability (ALMisned et al., 2024b).

2.2 Geant4 Simulation Setup

The Geant4 simulation toolkit was utilized to calculate the macroscopic neutron removal cross-sections, thus providing detailed insights into the interaction of neutrons with aluminum oxynitride (AlON). Geant4 is a versatile and widely used simulation program that is particularly effective for modeling particle interactions across various domains, including nuclear physics, space science, high-energy physics, and accelerator physics (Agostinelli et al., 2003; Allison et al., 2006, 2016). The flexibility and precision of the tool make it an invaluable resource for optimizing the design and performance of

high-budget experiments. In this study, the simulation setup involved a detailed definition of the geometry of the test material. This included the specification of all constituent elements, compounds, or mixtures, along with the material's density, physical state, and spatial configuration relative to the neutron source. The accurate representation of AlON was achieved by incorporating 23 Al, 27 O, and 5 N atoms into the simulation model, with a density of 3.67 g/cm^3 as reported in the literature (Johnson et al., 2012; Salifu and Olubambi, 2023). The experimental conditions were set to reflect typical room temperature and atmospheric pressure conditions, with the material in its solid state, in order to ensure that the simulation closely mimicked real-world conditions. The parameters used in simulations are given in Table 3. The SHIELDING physics list from Geant4 was selected for the simulations, a choice particularly suitable for neutron shielding studies due to its comprehensive treatment of neutron interactions. The physics list includes models for elastic and inelastic scattering, absorption, and capture, thus providing a robust framework for the analysis of neutron attenuation.

Table 3. Geant4 simulation parameters for AlON

Property	Value
Chemical Formula	$Al_{(64+x)/3}O_{(32-x)}N_x \quad (0 \leq x \leq 8)$
Most Stable Form ($x = 5$)	$Al_{23}O_{27}N_5$
Density	3.67 g/cm^3
Elemental Mass Fraction	55.28% Al, 38.48% O, 6.24% N
Elemental Abundance	41.82% Al, 49.09% O, 9.09% N

A critical aspect of the simulation was the configuration of the neutron source. The source was positioned 5 cm from the target, designed with a radius of 0.5 cm and a beam spread of 0.2 mm, directed along the +z axis. To achieve a narrow, focused beam, which is common in neutron shielding research, a beam-type source was utilized instead of a collimated point source. This approach ensures that the neutron flux impinging the target material is consistent with experimental setups typically used in neutron shielding studies. The simulation was run with 1,000,000 events per scenario to ensure statistical significance. This large number of events allows for a detailed analysis of neutron interactions within AlON, providing precise macroscopic neutron removal cross-sections. The high granularity of the data obtained from these simulations enables a thorough understanding of AlON's effectiveness as a neutron shielding material, which is crucial for its potential applications in nuclear and space environments. Moreover, post-simulation data analysis focused on evaluating the neutron attenuation characteristics of AlON across a range of neutron energies. The results were benchmarked against other common shielding materials, such as lead, water and standard concrete, to assess AlON's relative performance. This comparison highlights the strengths and limitations of AlON in practical shielding scenarios, offering valuable insights for its application in environments where neutron radiation is a concern.

The simulation for neutron removal cross-sections prepared with Geant4 is shown in Figure 1. In this figure, the red block represents the AlON material, which serves as the primary target for the neutron beam. The large blue block immediately behind it indicates the region where the energy losses of neutrons, after passing through the material, are recorded. This region is crucial for determining the degree of interaction the neutrons undergo as they traverse the AlON target. The green lines in the figure represent the neutrons that are sent in a well-collimated beam, ensuring a focused and uniform interaction with the target material. The simulation is designed to capture and record all possible interactions of neutrons with the material, including scattering, absorption, and transmission without interaction. Each of these interactions is significant as they contribute to the overall understanding of how AlON interacts with neutron radiation. However, for the specific calculation of neutron removal cross-sections, as defined in the literature, only the neutrons that pass through the material without any interaction are considered relevant (El-Khayatt, 2010). These non-interacting neutrons are essential for calculating the macroscopic removal cross-section, which is a measure of the material's effectiveness in attenuating or filtering out neutron radiation. Furthermore, the data recorded in the blue block is analyzed to determine the energy distribution of neutrons post-interaction, which provides insight into the material's shielding capabilities. The energy losses are directly related to the material's ability to absorb or scatter neutrons, which is critical for applications where neutron attenuation is required, such as in radiation shielding or nuclear reactors. By comparing the number of neutrons that pass through the material without interaction to the total number of neutrons sent in the beam, the macroscopic neutron removal cross-section can be accurately calculated, offering a quantitative measure of AlON's neutron shielding effectiveness.

These comprehensive simulations not only help in predicting the material's performance in various neutron-rich environments but also provide a basis for optimizing the material's composition and thickness to achieve desired neutron attenuation characteristics.

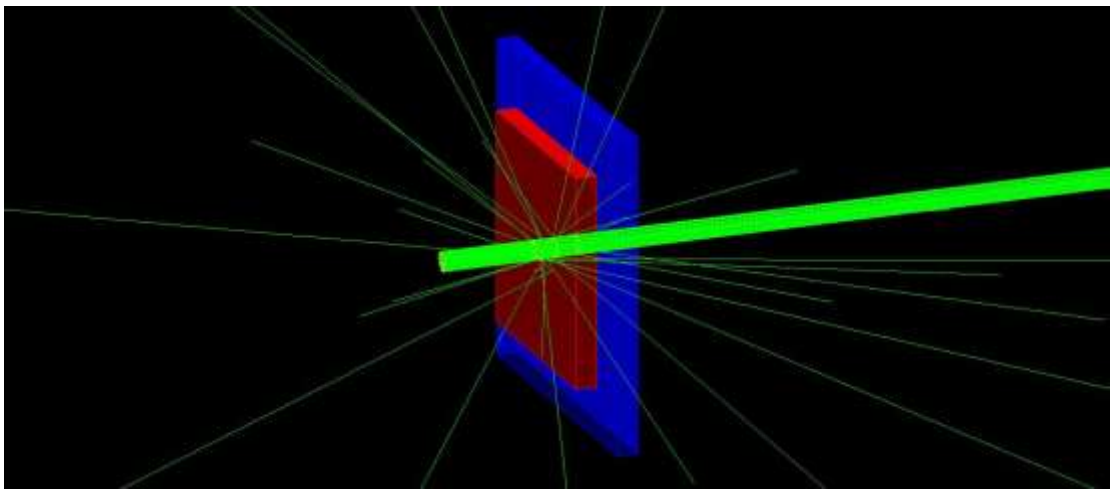

Figure 1. The image of the Geant4 simulation geometry. The red block presents the aluminum oxynitride while the blue block presents the neutron detector. The green lines represents the neutron beam. The incident and outgoing neutron flux can clearly be clearly seen in the figure.

3. Results and Discussion

In the study, the effectiveness of transparent aluminum oxynitride in stopping fast and thermal neutrons was calculated using conventional radiation attenuation parameters. As described in Section 2, the macroscopic neutron removal cross-section of AlON was calculated for different energies and thicknesses. Subsequently, for a fixed thickness and energy, the cross-sections of each element constituting AlON were considered, and the sum of these cross-sections was compared with the directly calculated cross-section.

First, we analyze the change in neutron removal cross-sections with increasing energy for fast neutrons. The graph shown in Figure 2 illustrates the variation of cross-sections with energy. Given that the neutrons in question are fast, the energy range is 2 to 10 MeV. The cross-sections obtained by varying the energy with 0.5 MeV intervals are plotted on the graph. As previously discussed, a larger macroscopic cross-section or a smaller transmission factor indicates superior shielding. As illustrated in Figure 2, while an increase in neutron energy is typically associated with a reduction in the macroscopic cross-section, the graph reveals a number of instances where the cross-section exhibits a sudden rise at specific intermediate energy values. For example, the macroscopic cross-section reaches its maximum value at approximately 3.5 MeV, after which it begins to decline and reaches a second maximum at approximately 6 MeV. These points may be indicative of resonance points for neutron capture or peak points for neutron scattering.

Expanding on the data in Figure 2, Figure 3 presents the variation in fast neutron removal cross-sections with respect to material thickness for selected neutron energy values. As seen in Figure 2, the values for 4 MeV and 6 MeV are lower than those for 3 MeV and 5 MeV, respectively. Here, since the vertical axis represents the transmission factor instead of the macroscopic removal cross-section, lower values correspond to better shielding properties. As an example, the removal cross-section values calculated for a neutron energy of 2 MeV are given in Table 4.

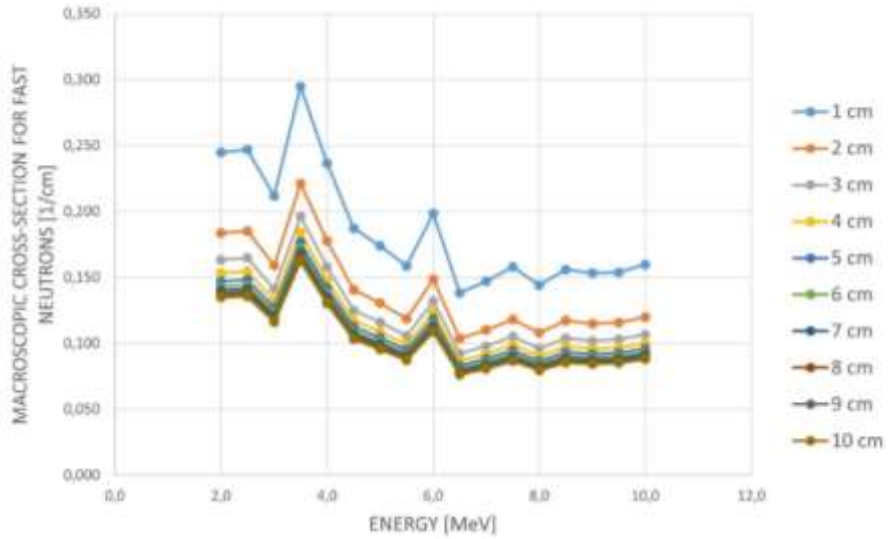

Figure 2. Comparison of macroscopic fast neutron cross-sections with increasing neutron energy.

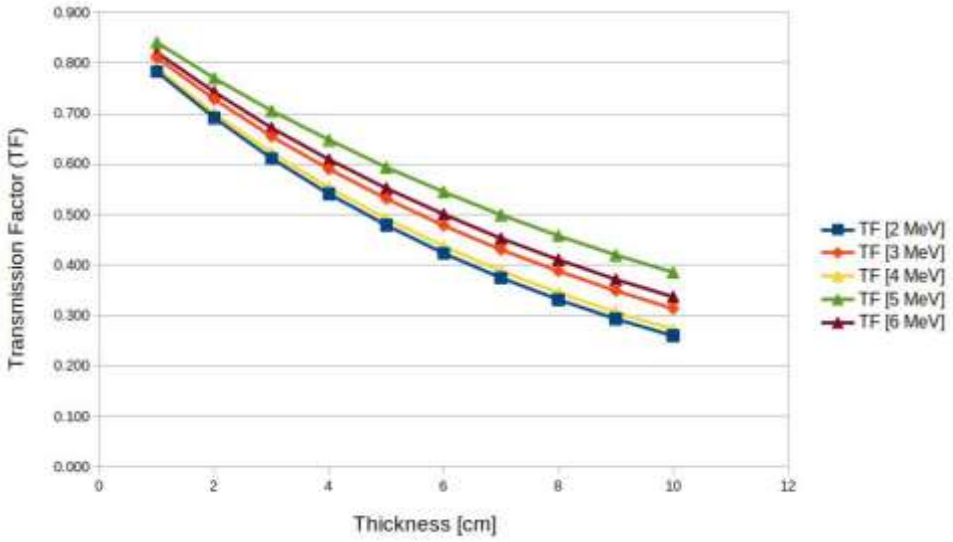

Figure 3. Comparison of transmission factors (TFs) with increasing target thickness. The graph also shows the effect of the neutron energy.

Table 4. The table shows the Macroscopic Neutron Removal Cross-Section for transparent aluminum oxynitride. It shows cross-section values for only 2 MeV neutron energy

Macroscopic Neutron Removal Cross-Section for 2 MeV										
Thickness [cm]	1	2	3	4	5	6	7	8	9	10
Cross-Section [1/cm]	0.245	0.184	0.163	0.153	0.147	0.143	0.140	0.138	0.136	0.135

For thermal neutrons, the TF values for AlON range from 0.663 to 0.104, proportional to the material thickness (lower values indicate better shielding). As expected, the best result is obtained at a thickness of 10 cm with a TF value of 0.104, whereas this value is 0.026 for concrete and 0.125 for lead. The same value is calculated as 0.000014 for water. Similarly, when AlON is evaluated for fast neutrons (2 MeV) over a thickness range of 1 to 10 cm, the TF values range from 0.783 to 0.260 (again, lower values indicate better shielding). These values are very close to the values calculated for water, which are 0.782 to 0.257, and it has been observed that AlON provides better shielding than both lead and concrete. As shown in Figure 4, water and AlON behave almost identically.

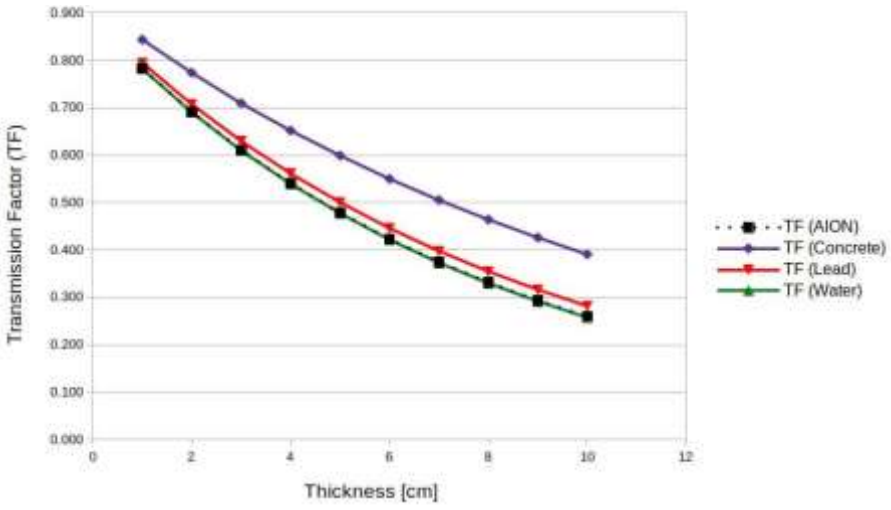

Figure 4. A comparison of conventional shielding materials with aluminum oxynitride for fast neutrons. The y-axis displays the transmission factor. In the case of fast neutrons, AlON is superior to concrete and lead, and is almost identical to water.

The last two graphs in this section compare the shielding capabilities of thermal and fast neutrons with other conventional shielding materials. First, the shielding capacity of AlON against fast neutrons is shown in Figure 4. In Figure 4, the change in the transmission factor with material thickness is shown for a constant fast neutron energy (2 MeV). Here, the neutron shielding capacity of AlON is compared with three other materials: concrete,

lead, and water. Their thicknesses were varied between 1 and 10 cm and compared with AlON. As can be seen in Figure 4, AlON provides superior performance in stopping fast neutrons compared to both concrete and lead. However, it yields nearly the same transmission factors as water. This indicates that AlON is a suitable material for neutron shielding when fast neutrons are concerned.

The graph in Figure 5 is an adaptation of the comparison for fast neutrons to thermal neutrons. The first noticeable feature is that AlON's excellent shielding performance for fast neutrons is not observed for thermal neutrons. Although it still provides better shielding than lead, it performs worse than both concrete and water.

According to the comparisons, transparent aluminum oxynitride demonstrates excellent shielding properties against fast neutrons but not for thermal neutrons. AlON, which provides better values than lead for thermal neutrons, may not be sufficient alone to stop or attenuate these neutrons. Neutron shielding has a more complex mechanism compared to gamma shielding and involves slowing down fast neutrons to thermal neutrons and then absorbing them to stop them (Ouardi, 2021). Therefore, ALON can be used either alone or as the initial shielding material to stop fast neutrons, depending on the application and conditions. The resulting thermal neutrons can then be stopped using a secondary material.

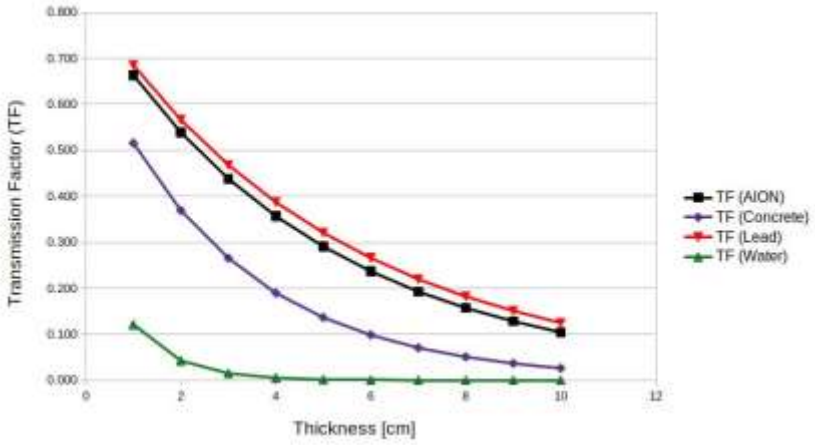

Figure 5. The figure presents the comparison of the four materials. Three of them are conventional radiation shielding materials while the third one is novel aluminum oxynitride. The AlON is superior to lead but worse than ordinary portland concrete and water for thermal neutrons.

4. Conclusion

This study investigated the neutron shielding effectiveness of transparent aluminum oxynitride (AlON) using a Geant4 Monte Carlo simulation. The macroscopic neutron removal cross-sections were calculated for various neutron energies and material thicknesses to assess AlON's performance. The results demonstrate that AlON has a high capacity for shielding fast neutrons, outperforming traditional materials like concrete and lead, and showing nearly identical performance to water. However, AlON's effectiveness in shielding thermal neutrons is more limited, only surpassing lead but falling short compared to concrete and water. Figures 4 and 5 further illustrate these findings. As shown in Figure 4, AlON proves superior to both concrete and lead in shielding fast neutrons, with performance almost equivalent to that of water. Conversely, Figure 5 reveals that while AlON outperforms lead in thermal neutron shielding, it does not match the effectiveness of Ordinary Portland Concrete or water. These findings suggest that AlON is a promising candidate for fast neutron shielding in various nuclear and radiation protection applications. However, its limited effectiveness against thermal neutrons highlights the potential need for a dual-material approach, where AlON could be combined with other materials to enhance overall neutron shielding efficiency.

While this study has provided valuable insights, several limitations must be acknowledged. The simulation results are contingent on the accuracy of the input parameters and the assumptions made, such as material purity and homogeneity. In real-world applications, these factors may vary, potentially affecting the material's performance. Future research could explore these limitations by conducting experimental validation of the simulation results and investigating the effects of impurities and material variations on AlON's shielding properties. Furthermore, studies could explore the potential of combining AlON with other materials to develop hybrid shielding solutions that offer enhanced protection against both fast and thermal neutrons.

Author Contributions

The percentages of the author contributions are presented below. The author reviewed and approved the final version of the manuscript.

	A.Y.
C	100
D	100
S	100
DCP	100
DAI	100
L	100
W	100
CR	100
SR	100
PM	100
FA	100

C=Concept, D= design, S= supervision, DCP= data collection and/or processing, DAI= data analysis and/or interpretation, L= literature search, W= writing, CR= critical review, SR= submission and revision, PM= project management, FA= funding acquisition.

Conflict of Interest

The author declared that there is no conflict of interest.

Ethical Consideration

Ethics committee approval was not required for this study because of there was no study on animals or humans.

References

Agostinelli S, Allison J, Amako KA, Apostolakis J, Araujo H, Arce P. 2003. Geant4 - a simulation toolkit. Nucl Instrum Methods Phys Res A, 506(3): 250-303.

Akyıldırım H. 2019. Calculation of fast neutron shielding parameters for some essential carbohydrates. Erzincan Üniv Fen Bilim Enst Derg, 12(2): 1141-1148.

Al-Buriahi M, Bakhsh EM, Tonguc B, Khan SB. 2020. Mechanical and radiation shielding properties of tellurite glasses doped with ZnO and NiO. Ceram Int, 46(11): 19078-19083.

Ali MS, Hassan GS, Shoraiet GM, Abdelmonem AM. 2024. Optimizing gamma-ray shielding for boron neutron capture therapy by using unglazed ceramic composites. Nucl Instrum Methods Phys Res B, 554: 165450.

Allison J, Amako K, Apostolakis J, Araujo H, Dubois PA, Asai M. 2006. Geant4 developments and applications. IEEE Trans Nucl Sci, 53(1): 270-278.

Allison J, Amako K, Apostolakis J, Arce P, Asai M, Aso T. 2016. Recent developments in geant4. Nucl Instrum Methods Phys Res A, 835: 186-225.

AlMisned G, Sen Baykal D, Elshami W, Susoy G, Kilic G, Tekin HO. 2024a. A comparative analysis of shielding effectiveness in glass and concrete containers. Open Phys, 22(1): 20240019.

AlMisned G, Susoy G, Tekin H. 2024b. Neutron transmission analysis in borated polyethylene, boron carbide, and polyethylene: Insights from MCNP6 simulations. Radiat Phys Chem, 218: 111585.

AlMisned G, Tekin HO, Kavaz E, Bilal G, Issa SA, Zakaly HM, Ene A. 2021. Gamma, fast neutron, proton, and alpha shielding properties of borate glasses: a closer look on lead (ii) oxide and bismuth (iii) oxide reinforcement. Appl Sci, 11(15): 6837.

Alomayrah N, Alrowaili Z, Alalawi A, Al-Buriahi M. 2024. Gamma and neutron attenuation of asm geopolymers for radiation shielding applications: Theoretical study. J Radiat Res Appl Sci, 17(2): 100876.

Alrowaili ZA, Alsaiari NS, İbrahimoğlu E, Çalışkan F, Olarinoye IO, Al-Buriahi MS. 2024. Physical, chemical and radiation shielding properties of metakaolin-based geopolymers containing borosilicate waste glass. Radiat Phys Chem, 224: 112075.

Alzahrani FMA, Basha B, Hammoud A, Tamam N, Alsufyani SJ, Kebaili I. 2024a. Gamma attenuation and nuclear shielding ability of 〖TeO〗_2/〖Bi〗_2 O_3/〖WO〗_3 glass system. Radiat Phys Chem, 223: 111985.

Alzahrani JS, Alrowaili ZA, Alalawi A, Alshahrani B, Al-Buriahi MS. 2024b. Gamma and neutron attenuation of 〖Bi〗_2 O_3/CaO modified borovanadate glasses for radiation shielding applications. J Radiat Res Appl Sc, 17: 100887.

Alzahrani JS, Alrowaili ZA, Sriwunkum C, Al-Buriahi MS. 2024c. Radiation and nuclear shielding performance of tellurite glass system containing 〖Li〗_2 O and MoO_3: XCOM and FLUKA Monte Carlo. J Radiat Res Appl Sc, 17: 100923.

Cherkashina N, Pavlenko V, Shkaplerov A, Kuritsyn A, Sidelnikov R, Popova E, Umnova LA, Domarev S. 2024. Neutron attenuation in some polymer composite material. Adv Space Res, 73(5): 2638-2651.

El-Khayatt A. 2010. Calculation of fast neutron removal cross-sections for some compounds and materials. Ann Nucl Energy, 37(2): 218-222.

Fahmi AHM, Sazali MA, Yazid K, Bakar AAA, Ali NSM, Jamaluddin K, Sarkawi MS. 2024. Analysis of graphite-paraffin composite in neutron radiography, impact resistance, and thermal neutron attenuation. Radiat Phys Chem, 218: 111639.

Gaylan Y, Bozkurt A, Avar B. 2021. Investigating thermal and fast neutron shielding properties of b4c, b2o3, sm2o3, and gd2o3 doped polymer matrix composites using Monte Carlo simulations. Süleyman Demirel Üniversitesi Fen Edebiyat Fakültesi Fen Dergisi, 16(2): 490-499.

Johnson R, Biswas P, Ramavath P, Kumar R, Padmanabham G. 2012. Transparent polycrystalline ceramics: an overview. T Indian Ceram Soc, 71(2): 73-85.

Kaçal M, Akman F, Sayyed M. 2019. Evaluation of gamma-ray and neutron attenuation properties of some polymers. Nucl Eng Technol, 51(3): 818-824.

Katubi KM, İbrahimoğlu E, Çalışkan F, Alrowaili ZA, Olarinoye IO, Al-Buriahi MS. 2024. Apatite–Wollastonite (AW) glass ceramic doped with B_2 O_3: Synthesis, structure, SEM, hardness, XRD, and neutron/charged particle attenuation properties. Ceram Int, 50: 27139-27146.

Kim J, Lee BC, Uhm YR, Miller WH. 2014. Enhancement of thermal neutron attenuation of nano-b4c,-bn dispersed neutron shielding polymer nanocomposites. J Nucl Mater, 453(1-3): 48-53.

Lakshminarayana G, Tekin HO, Dong M, Al-Buriahi M, Lee DE, Yoon J, Park T. 2022. Comparative assessment of fast and thermal neutrons and gamma radiation protection qualities combined with mechanical factors of different borate-based glass systems. Results Phys, 37: 105527.

Li X, Cui D, Zou C, Ren C, Chen J. 2024. Neutron shielding analysis for a gadolinium doped nickel alloy. Mater Today Commun, 38: 107933.

Ouardi A. 2021. Neutron shielding calculations for neutron imaging facility at the maamora triga reactor. Appl Radiat Isotopes, 176: 109852.

Özdoğan H, Üncü YA, Akman F, Polat H, Kaçal MR. 2024. Detailed analysis of gamma-shielding characteristics of ternary composites using experimental, theoretical and Monte Carlo simulation method. Polymers, 16:1778.

Pavlenko V, Edamenko O, Cherkashina N, Kuprieva O, Noskov A. 2015. Study of the attenuation coefficients of photon and neutron beams passing through titanium hydride. J Surf Investig, 9: 546-549.

Pianpanit T, Saenboonruang K. 2024. Understanding neutron-shielding properties of self-healing poly (vinyl alcohol) hydrogels containing rare-earth oxides through simulations. Results Phys, 57: 107436.

Ramisetty M, Sastri S, Kashalikar U, Goldman LM, Nag N. 2013. Transparent polycrystalline cubic spinels protect and defend. Am Ceramics Soc Bull, 92(2): 20-25.

Reda AM, Ahmed R, Alsawah MA, El-Sabbagh SH, Elabd AA, Kansouh W. 2024. Radiation shielding effectiveness, structural, and mechanical properties of hdpe/b4c composites reinforced with fe2o3-al2o3-al-fe fillers. Phys Scr, 99: 035308.

Salifu S, Olubambi PA. 2023. Transparent aluminium ceramics: fabrication techniques, setbacks and prospects. J Korean Ceram Soc, 60(1): 24-40.

Singh VP, Badiger N. 2014. Gamma ray and neutron shielding properties of some alloy materials. Ann Nucl Energy, 64: 301-310.

Singh VP, Badiger N, Chanthima N, Kaewkhao J. 2014. Evaluation of gamma ray exposure buildup factors and neutron shielding for bismuth borosilicate glasses. Radiat Phys Chem, 98: 14-21.

Tellili B, Elmahroug Y, Souga C. 2014. Calculation of fast neutron removal cross sections for different lunar soils. Adv Space Res, 53(2): 348-352.

Yıldırım A. 2024. Radiation attenuation properties of transparent aluminum oxynitride: a comprehensive study. Eur Phys J Plus, 139(5): 383.

Zayed AM, El-Khayatt AM, Mahmoud KA, Petrounias P, Masoud MA. 2024. Evaluation of some heavyweight minerals as sustainable neutron and gamma-ray attenuating materials: comprehensive theoretical and simulation investigations. Arab J Sci Eng, Early Access, https://doi.org/10.1007/s13369-024-09300-2.